PCCP

ARTICLE TYPE

Cite this: DOI: 00.0000/xxxxxxxxxx

Supporting Information: Drained and undrained heat capacity of swelling clays

Tulio Honorio*[a] and Laurent Brochard[b]

Received Date
Accepted Date

DOI: 00.0000/xxxxxxxxxx

1 Vibrational density of states computed from the VACF

We develop the demonstration of the expression of the vibrational density of states (VDOS). We also provide details on how to compute the VDOS from the velocity autocorrelation function (VACF) in classical MD simulations. The demonstration is based on Dickey and Paskin[1] but taking into account the mass, and using the equipartition theorem to address the case of different masses.

Let us consider the steady state motion of atoms as the superposition of $3N$ harmonic oscillators of pulsation ω_i:

$$u_j(t) = \sum_i A_i^j \cos(\omega_i t + \phi_i^j) \Rightarrow v_j(t) = \sum_i A_i^j \omega_i \sin(\omega_i t + \phi_i^j) \quad (1)$$

The mass weighted VACF is defined as the average of $m_j v_j(t+t_0).v_j(t_0)$ over all initial time and all atoms:

$$\mathrm{VACF}(t) = \frac{1}{N}\sum_{j=1}^{N} \lim_{T\to\infty} \frac{1}{T}\int_0^T m_j v_j(t+t_0).v_j(t_0)dt_0 \quad (2)$$

For simplicity, we use the notation: $\mathrm{VACF}(t) = \left\langle m_j v_j(t+t_0).v_j(t_0)\right\rangle_{t_0,j}$.

Introducing the superposition of harmonic oscillators, we have:

$$\mathrm{VACF}(t) = \left\langle \sum_i m_j (A_i^j \omega_i)^2 \sin(\omega_i(t+t_0)+\phi_i^j).\sin(\omega_i t_0 + \phi_i^j)\right\rangle_{t_0,j} \quad (3)$$

The vibrational modes are orthogonal (see Dove[2] for this point), which explains why no term with $A_i^j A_i^k$ $(j \neq k)$ appears.

Averaging over all initial times leads to

$$\mathrm{VACF}(t) = \sum_i \frac{m_j \langle (A_i^j \omega_i)^2\rangle_j}{2}\cos(\omega_i t) \quad (4)$$

According to the equipartion theorem, the average kinetic energy of an harmonic oscillator is $kT/2$:

$$\left\langle \frac{m_j (A_i^j \omega_i)^2}{2}\right\rangle_j = \frac{kT}{2} \quad (5)$$

therefore

$$\mathrm{VACF}(t) = \frac{kT}{2}\sum_i \cos(\omega_i t) \quad (6)$$

Considering the normalized VACF, we have:

$$\gamma(t) = \frac{\left\langle m_j v_j(t+t_0).v_j(t_0)\right\rangle_{t_0,j}}{\left\langle m_j v_j(t_0).v_j(t_0)\right\rangle_{t_0,j}} = \frac{\frac{kT}{2}\sum_i \cos(\omega_i t)}{3N\frac{kT}{2}} = \frac{1}{3N}\sum_i \cos(\omega_i t) \quad (7)$$

Introducing the vibrational density of states as:

$$\sum_i \cos(\omega_i t) = \int_{-\infty}^{+\infty} \rho(\omega)\cos(\omega t)d\omega \quad (8)$$

or

$$\gamma(t) = \int_{-\infty}^{+\infty} \frac{\rho(\omega)}{3N}\cos(\omega t)d\omega = \int_{-\infty}^{+\infty} g(\omega)\cos(\omega t)d\omega = \Re[\mathscr{F}(f)] \quad (9)$$

The normalized mass weighted VACF $\gamma(t)$ is the real part of the Fourrier transform of the normalized VDOS $g(\omega) = \frac{\rho(\omega)}{3N}$:

$$\gamma(t) = \int_{-\infty}^{+\infty} g(\omega)\frac{e^{i\omega t}+e^{-i\omega t}}{2}d\omega = \int_{-\infty}^{+\infty}\frac{g(\omega)+g(-\omega)}{2}e^{i\omega t}d\omega \quad (10)$$

that is

$$\gamma(t) = 2\pi\mathscr{F}^{-1}\left(\frac{g(\omega)+g(-\omega)}{2}\right) \quad (11)$$

Therefore, $\frac{\gamma(t)}{2\pi}$ is the inverse Fourrier transform of the symetrized VDOS $\frac{f(\omega)+f(-\omega)}{2}$. Inverting the expression above, we

[a] Université Paris-Saclay, CentraleSupélec, CNRS, LMPS - Laboratoire de Mécanique Paris-Saclay, 91190, Gif-sur-Yvette, France. Fax: +33(0)1 81 87 51 02; Tel: +33(0)1 81 87 51 02; E-mail: tulio.honorio-de-faria@ens-paris-saclay.fr
[b] Laboratoire Navier, Ecole des Ponts ParisTech, Univ Gustave Eiffel, CNRS, Marne-la-Vallée, France.

get:

$$\frac{g(\omega)+g(-\omega)}{2} = \int_{-\infty}^{+\infty} \frac{\gamma(t)}{2\pi} e^{-i\omega t} dt \quad (12)$$

Since the VDOS contains only positive pulsations, we limit ourselves to $\omega > 0$ and $g(-\omega) = 0$, so that:

$$g(\omega) = \frac{1}{\pi} \int_{-\infty}^{+\infty} \gamma(t) e^{-i\omega t} dt \quad (13)$$

Since the VACF is reversible in time (Newton's law is reversible), $\gamma(t) = \gamma(-t)$ so that it guarantees the result is real:

$$g(\omega) = \frac{1}{\pi} \int_{0}^{+\infty} \gamma(t)(e^{i\omega t} + e^{-i\omega t}) dt = \frac{2}{\pi} \int_{0}^{+\infty} \gamma(t)\cos(\omega t) dt \quad (14)$$

2 Hybrid GCMC-NVT simulations

Hybrid GCMC-NVT simulations are performed to obtained configurations with the water content corresponding to equilibrium at 300 K and RH of 100%.

These simulations are perfomed to sample the Grand canonical ensemble (μVT) for water while keeping the number of atoms in the solid layers and Na or Ca counterions constant. The GCMC stage enables the exchange of water molecules with an infinite reservoir at imposed chemical potential and temperature. We adopt a chemical potential corresponding to an RH of 100% (i.e. the water pressure P_w to be imposed is the liquid-vapor coexistence pressure, which is 0.01004 atm for SPC/E water at 300 K[3]). The NVT stage enable us to gain in computational efficiency by better sampling the phase space. Counterions are time integrated during the NVT run, while particles in the solid are not. Water molecules are constrained with SHAKE algorithm.

The total of 5 million Monte Carlo moves were enough to equilibrate all system studied according to the total energy and particle number variations. Then, a simulation comprising 10 million Monte Carlo moves was used for production.

In these hybrid simulations, the effects of the deformation of the solid lattice due to the thermal expansion or compression should be minor since the thermal expansion and compressibility of fluids (confined fluids included) are expected to be much larger than that of solids. The NVT simulation, with flexible solid lattice, performed over the final configuration of GCMC returns thermodynamic data that are in agreement with GCMC results.

3 Heat capacity

3.1 Semi-classical estimates

Figures 1 and 2 show the normalized velocity auto-correlation function (VACF) $\langle \mathbf{v}_j(t).\mathbf{v}_j(0)\rangle / \langle \mathbf{v}_j(0)^2\rangle$ and the mass-weighted VACF $\langle m\mathbf{v}_j(t).\mathbf{v}_j(0)\rangle / \langle \mathbf{v}_j(0)^2\rangle$ obtained from NVE simulations. The figure shows that integration up to 10 picoseconds is enough to capture the decay in the VACFs.

Figure 3 shows the vibrational density of states (VDOS) $g(\omega)$ for a few selected cases. Frequencies up to 900 THz were considered in order to identify the range in which the VDOSs do not vanish. Considering frequencies up to ω=100 THz is enough to capture the VDOS of both Na- and Ca-Mmt for all basal spacings considered.

Figure 4 shows the VDOS $g(\omega)$ for selected basal spacings for both Na- and Ca-Mmt in the range of frequencies up to 100 THz. These functions are integrated to obtain the semi-classical estimates in this work. We also show the specific contribution of water alone, and solid layers and counterions in (C)-(F).

3.2 Semi-classical estimates for bulk water

The normalized VACF, normalized mass-weighted VACF, and VDOS used to compute the semi-classical estimates of the heat capacity of bulk water are shown in Figure 5. Using Green-Kubo formula, (e.g.[4]), we check that the self-diffusion coefficient of water obtained fro the VACF is consistent with the values reported in previous studies. The VDOS shows remarkable good agreement with the peak positions reported in ref.[5].

3.3 (Classical) finite difference approach for the heat capacity of confined flexible SPC/E water

Figure 6 shows the comparison between the results of classical approaches using the fluctuation formula (Eq. 2) and finite difference (FD) approach. For the FD case, we use the definitions in Eq. 1. NVT simulations are performed at five temperatures: 280 K, 290 K, 300 K, 310 K, and 320 K. The same configurations equilibrated at 300 K, 1 atm, and RH of 100% for each basal spacing from the GCMC simulations are used in all cases as the initial configuration. For each basal spacing, a least-squares linear fitting is performed accounting for the five couples of temperature and internal energy, and C_v is obtained from the slope of that fitted line.

4 Effect of the mixing of hydration states in the heat capacity of clays

Regarding the effect of the mixing of hydration states under pressure control, we compare in Figure 7 the results of heat capacity (i) directly computed from MD (i.e. following the oscillatory profiles in Figure 1) and (ii) with estimates assuming a mix of hydration states in the unstable zones (i.e. following the stable path at depicted by the dashed lines representing the convex hull in Figure 2, we consider the metastable states, up to spinodal decomposition, in compression). Both cases yield similar results because of the almost linear evolution of the heat capacity with the basal spacing, even for small basal spacing.

5 Elastic constants

The stiffness tensor is computed from a finite-difference approach using the definition[4]:

$$\mathbf{C} = C_{ijkl} = \left[\frac{\partial \sigma_{ij}}{\partial \varepsilon_{kl}}\right]_{T,\varepsilon_{kl}} \quad (15)$$

The finite difference approach consists in slightly deforming (within the elastic domain) the simulation box in each one of the six axial and tangential directions followed by relaxation using Nosé-Hoover thermostat and barostat. Both negative and positive deformation are considered for each direction in order to avoid any asymmetric effect under loading.

In agreement with previous works[6], the in-plane elastic coeffi-

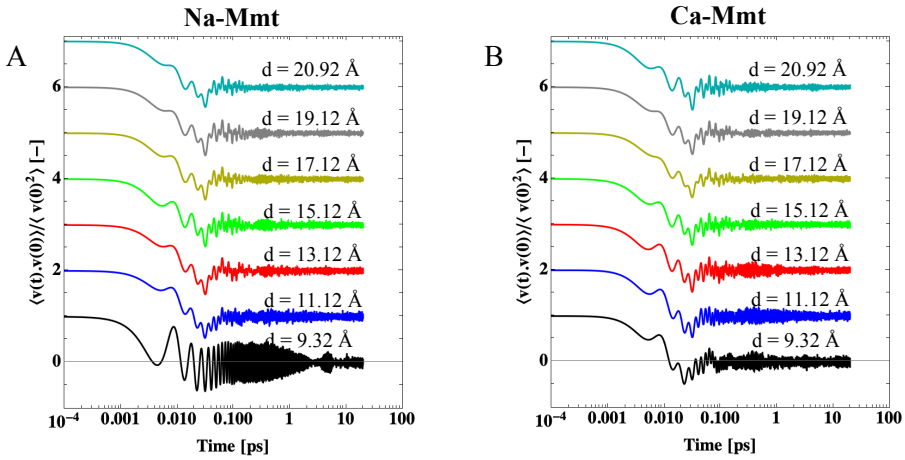

Fig. 1 Normalized VACF of (A) Na- and (B) Ca-Mmt for selected basal spacings.

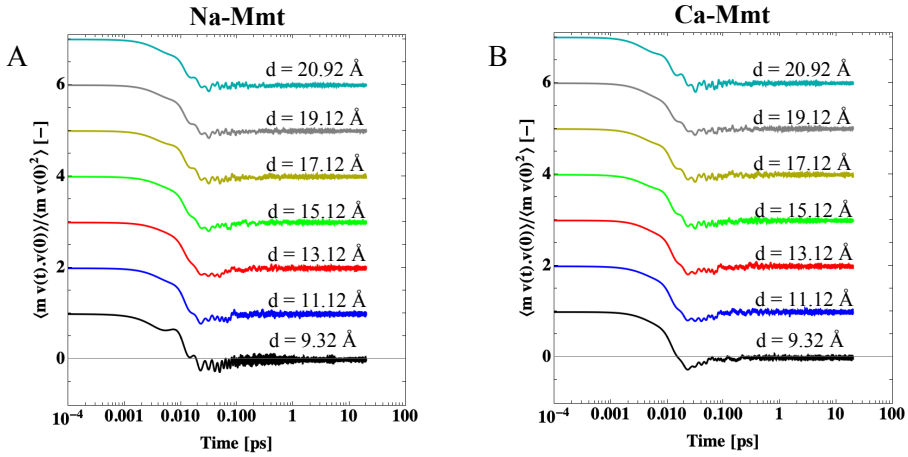

Fig. 2 Normalized mass VACF $\langle m\mathbf{v}_j(t).\mathbf{v}_j(0)\rangle/\langle \mathbf{v}_j(0)^2\rangle$ of (A) Na- and (B) Ca-Mmt for selected basal spacings.

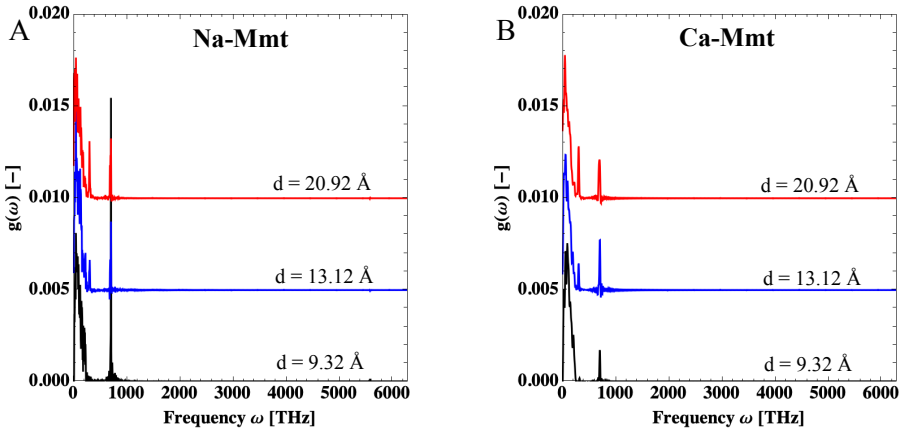

Fig. 3 Range of frequencies of the VDOS of (A) Na- and (B)-Mmt for selected basal spacings.

cient $C_{12} \approx C_{11}/2$; and the out-of-plane coefficient $C_{13} \approx C_{33}/2$.

The bulk modulus K can be directly computed using the fluctuation formula in an NσT simulation[4]:

$$\frac{1}{K} = \frac{\langle V^2\rangle_{N\sigma T} - \langle V\rangle^2_{N\sigma T}}{kTV}. \tag{16}$$

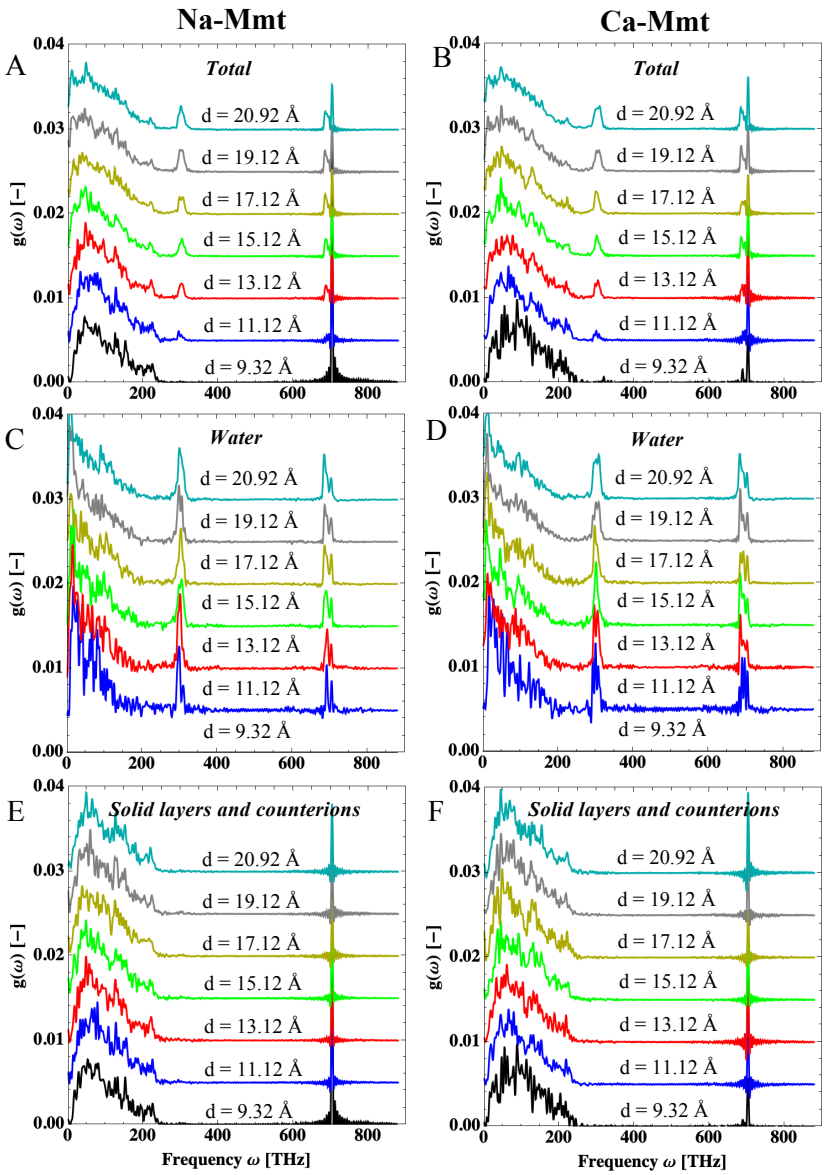

Fig. 4 VDOS of Na-Mmt (left) and Ca-Mmt (right) for selected basal spacings: (A) and (B) total VDOS, (C) and (D) water only; and (E) and (F) solid layers and counterions only.

6 Coefficient of thermal expansion

The full tensor of coefficients of thermal expansion α is computed using a fluctuation-dissipation approach in an isotension-isothermal (NσT) simulation[7–9]:

$$\alpha = \frac{\langle H\varepsilon\rangle_{N\sigma T} - \langle H\rangle_{N\sigma T}\langle\varepsilon\rangle_{N\sigma T}}{kT^2}. \quad (17)$$

where $\varepsilon = \frac{1}{2}\left[\mathbf{h}_0^{-T}\mathbf{h}^T\mathbf{h}\mathbf{h}_0^{-1} - \mathbf{I}\right]$ is the second-order Lagrangian deformation tensor obtained from the $\mathbf{h}$ matrix at the reference (subscript 0) and deformed states, $\mathbf{I}$ is the identity matrix, and the superscript $[\star]^T$ stands for the transpose operator.

Figure 9 shows the coefficients of thermal expansion as a function of the water content m_w/m_{total} of Na- and Ca-Mmt. The in-plane coefficients α_{xx} and α_{yy}, dominated by the expansion of the solid layers, do not show significant changes with respect to the water content. The average values are:

For Na-Mmt:

- α_{xx} = (0.98±0.18) $\times 10^{-5}$/K
- α_{yy} = (1.39±0.25) $\times 10^{-5}$/K.

For Ca-Mmt:

- α_{xx} = (0.89±0.31) $\times 10^{-5}$/K
- α_{yy} = (1.28±0.55) $\times 10^{-5}$/K.

Therefore, in-plane coefficients can be fairly considered as independent of the counterion type. This results is consistent with previous works reporting in-plane coefficients of thermal expansion independent on the hydration state and being $\alpha_{11} \approx \alpha_{22} = 1.0\pm 0.2 \times 10^{-5}$/K[6]. The out-of-plane coefficient α_{33} is reported

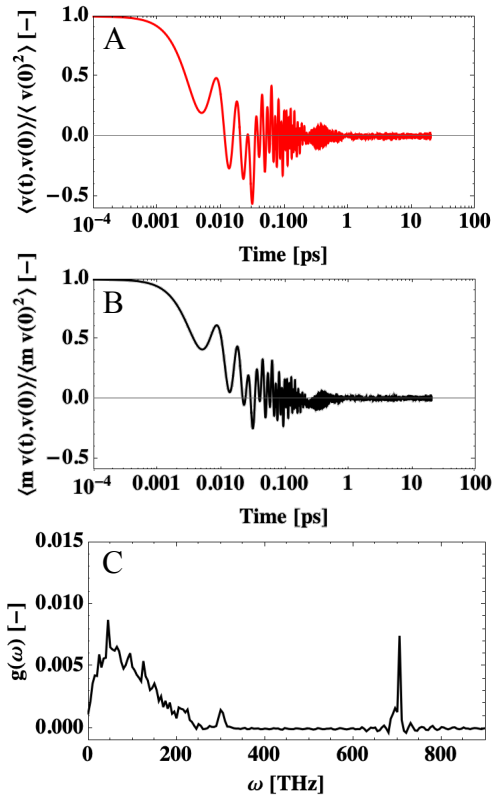

Fig. 5 (A) normalized VACF, (B) normalized mass-weighted VACF, and (C) VDOS of bulk water.

to be roughly three times the values of α_{11} or α_{22} [6], since the behavior in that direction is governed by liquid water expansion. Consistently, the coefficient of thermal expansion at the layer scale were experimentally obtained for other phyllosilicates such as muscovite (a mica) and are $\alpha_{11} = 0.83 \times 10^{-5}$ K^{-1}, $\alpha_{22} = 1.00 \times 10^{-5}$ K^{-1}, and α_{11} =2.13 $\times 10^{-5}$ K^{-1} [10].

The out-of-plane coefficient α_{zz} is computed using two approaches: (i) directly from the fluctuation of the deformations, and (ii) indirectly using the fluctuation of the volume $\alpha_v = \frac{\langle HV\rangle_{N\sigma T} - \langle H\rangle_{N\sigma T}\langle V\rangle_{N\sigma T}}{V_0 kT^2}$ and the values of of the in-plane coefficients: $\alpha_{zz} = \alpha_v - \alpha_{xx} - \alpha_{yy}$. The latter is less prone to variability in the simulations. Both estimates of α_{zz} are fitted with a linear function. The expected increasing trend of α with the water content is captured by the indirect method. Also, the indirect method leads to a better coefficient of determination The α_{zz} of Ca-Mmt exhibits a more pronounced increase with the water content than Na-Mmt.

7 Difference between heat capacity at constant pressure and heat capacity at constant volume

Figure 10 shows the difference between the heat capacity at constant pressure and the heat capacity at constant volume as a function of the water content m_w/m_{total}. The difference $C_p - C_v$ is computed using the full stiffness $\mathbf{C}$ and thermal expansion α tensors and using the bulk modulus K and volumetric coefficient of thermal expansion α_v (via the expression [4]: $C_p - C_v = K\alpha^2 T/\rho$, where the bulk modulus were obtained from a fluctuation formula in NσT ensemble as discussed here in the Supporting Material). The values $C_p - C_v$ obtained are consistent with results obtained for other phyllosilicates (e.g. circa 10 J/(kg.K) for calcium silicate hydrates at equilibrium basal spacing [12]).

Notes and references

1 J. M. Dickey and A. Paskin, *Physical Review*, 1969, **188**, 1407–1418.
2 M. T. Dove, *Introduction to Lattice Dynamics*, Cambridge University Press, 1993.
3 M. Fugel and V. C. Weiss, *The Journal of Chemical Physics*, 2017, **146**, 064505.
4 M. P. Allen and D. J. Tildesley, *Computer Simulation of Liquids*, Oxford University Press, New York, 1989.
5 P. H. Berens, D. H. J. Mackay, G. M. White and K. R. Wilson, *The Journal of Chemical Physics*, 1998, **79**, 2375.
6 B. Carrier, M. Vandamme, R. J.-M. Pellenq and H. Van Damme, *The Journal of Physical Chemistry C*, 2014, **118**, 8933–8943.
7 T. Cagin, N. Karasawa, S. Dasgupta and W. A. Goddard, *MRS Online Proceedings Library Archive*, 1992, **278**, year.
8 J. R. Ray, *The Journal of Chemical Physics*, 1983, **79**, 5128–5130.
9 T. Honorio, T. Lemaire, D. D. Tommaso and S. Naili, *Materialia*, 2019, 100251.
10 A. Pavese, G. Ferraris, V. Pischedda and R. Ibberson, *EUROPEAN JOURNAL OF MINERALOGY*, 1999, **11**, 309–320.
11 W. M. Haynes, *CRC Handbook of Chemistry and Physics, 95th Edition*, CRC Press, 2014.
12 M. J. A. Qomi, F.-J. Ulm and R. J.-M. Pellenq, *Physical Review Applied*, 2015, **3**, 064010.

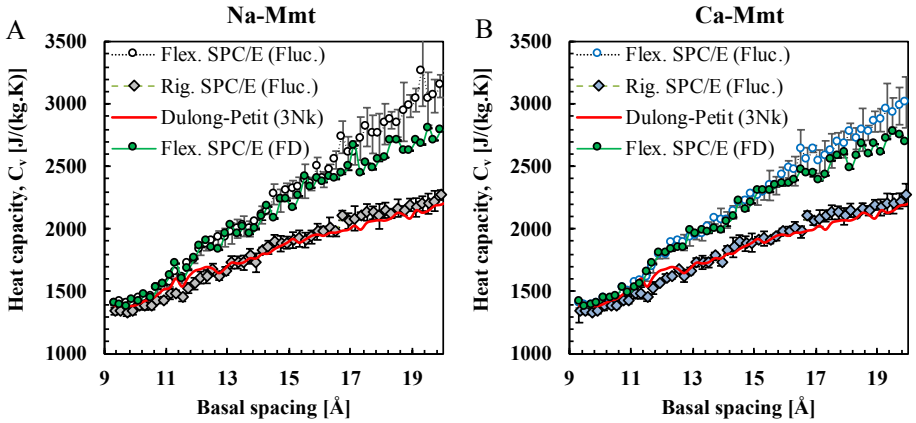

Fig. 6 Full classical computations of the undrained heat capacity C_v of (A) Na- and (B) Ca-Mmt as a function of basal spacing: comparison of results using fluctuation and finite difference (FD) methods.

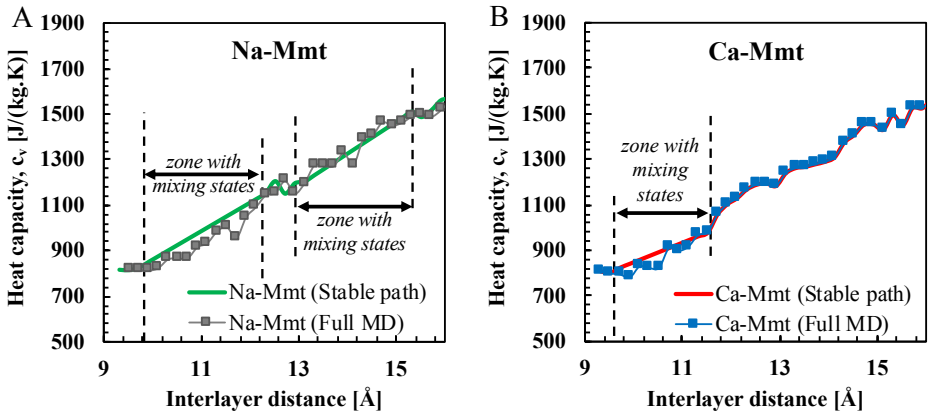

Fig. 7 Heat capacity as a function of the basal spacings: comparison of the results) directly computed from MD (i.e. following the oscillatory profiles in Figure 1 of the main text) with estimates assuming a mix of hydration states in the unstable zones (i.e. following the stable path at depicted by the dashed lines representing the convex hull in Figure 1 of the main text).

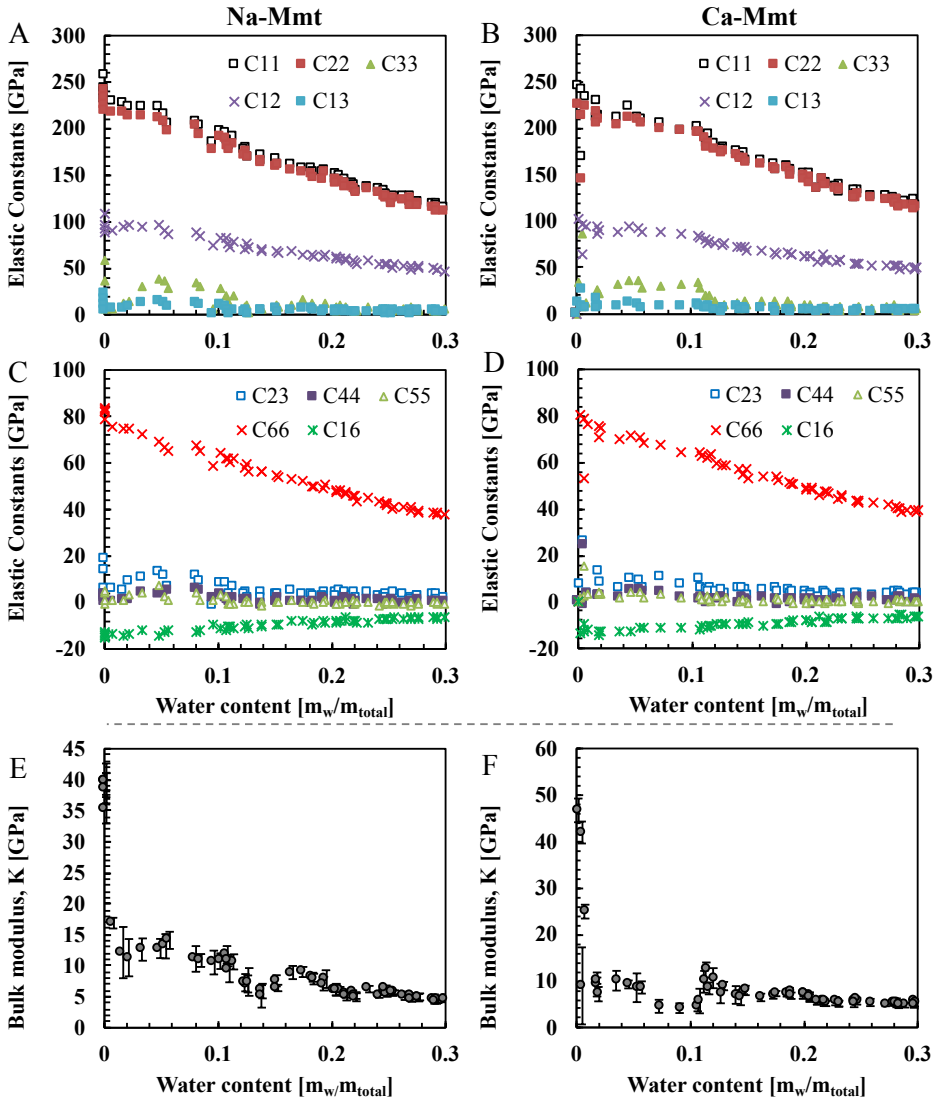

Fig. 8 (A)-(D) Elastic constants computed using a finite difference approach at 298 K for Na-Mmt (left) and Ca-Mmt (right). (E)-(F) Respective bulk modulus computed from fluctuation approach at NσT ensemble.

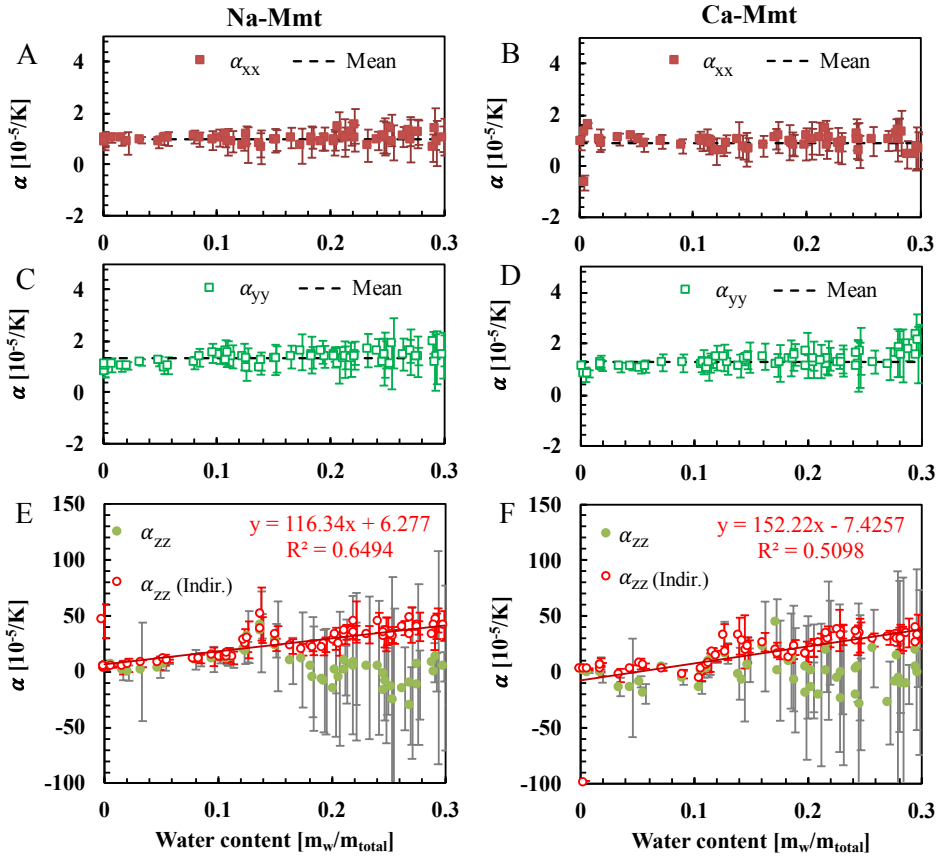

Fig. 9 Coefficients of thermal expansion as a function of the water content m_w/m_{total} of Na- and Ca-Mmt: (A)-(D) in-plane coefficients α_{xx} and α_{yy}, and (E)-(F) out-of-plane coefficient α_z. The experimental value for bulk water is α_v=20.6 $\times$ 10^{-5} K^{-1} [11].

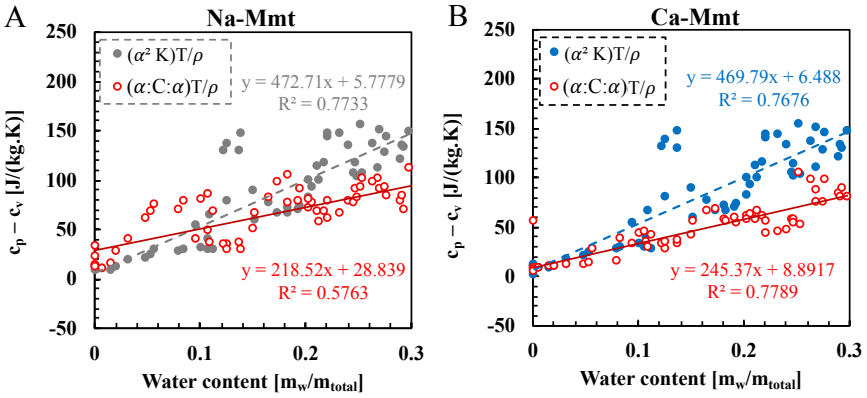

Fig. 10 Difference between the heat capacity at constant pressure and the heat capacity at constant volume as a function of the water content m_w/m_{total} for both Na- and Ca-Mmt. The difference $C_p - C_v$ is computed using the full stiffness $\mathbf{C}$ and thermal expansion α tensors (empty symbols) and using the bulk modulus K and volumetric coefficient of thermal expansion α_v (full symbols).The experimental value of $C_p - C_v$ is 43.7 J/(Kg.K) [11].